Supplementary Information

Supplementary Figure S1

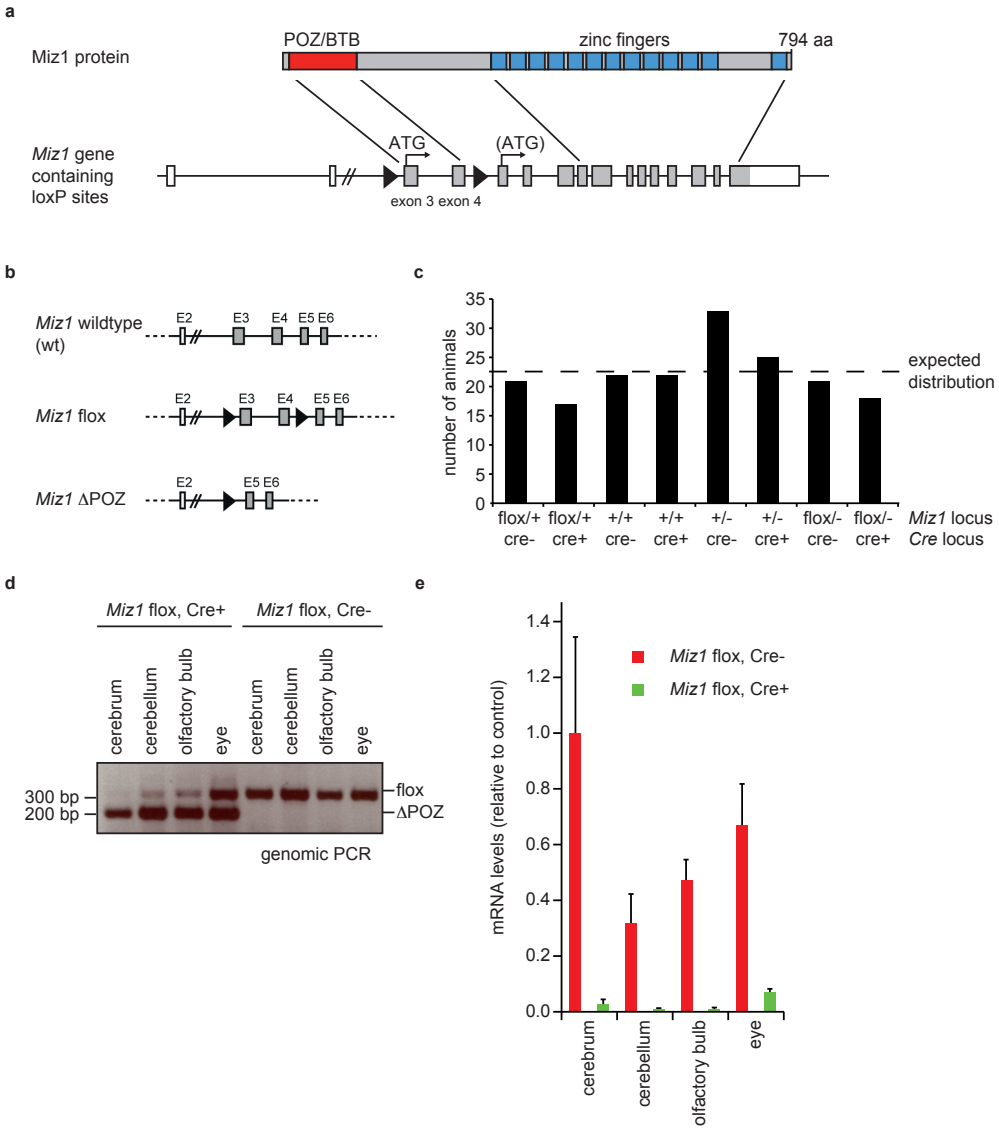

Supplementary Figure S1: Generation and characterization of *Miz1*$^{\Delta POZNes}$ mice.

(a, b) Scheme of the mouse models used. The amino-terminal POZ domain of Miz1 is encoded by exon 3 and exon 4, which are flanked by loxP sites (black triangles).

(c) *Miz1*$^{wt/\Delta POZ}$ and *Miz1*$^{flox/wtNes}$ mice were crossed and the number of offspring genotypes was analyzed (n = 179). The expected number of animals according to Mendelian laws is indicated.

(d, e) Expression of *Miz1* in different tissues from *Miz1*$^{\Delta POZNes}$ and control mice was tested by genomic PCR (d) and qRT-PCR (e). Primers are located within exons 3 and 4. The experiment was performed twice with identical results. Error bars are SD of three technical replicates.

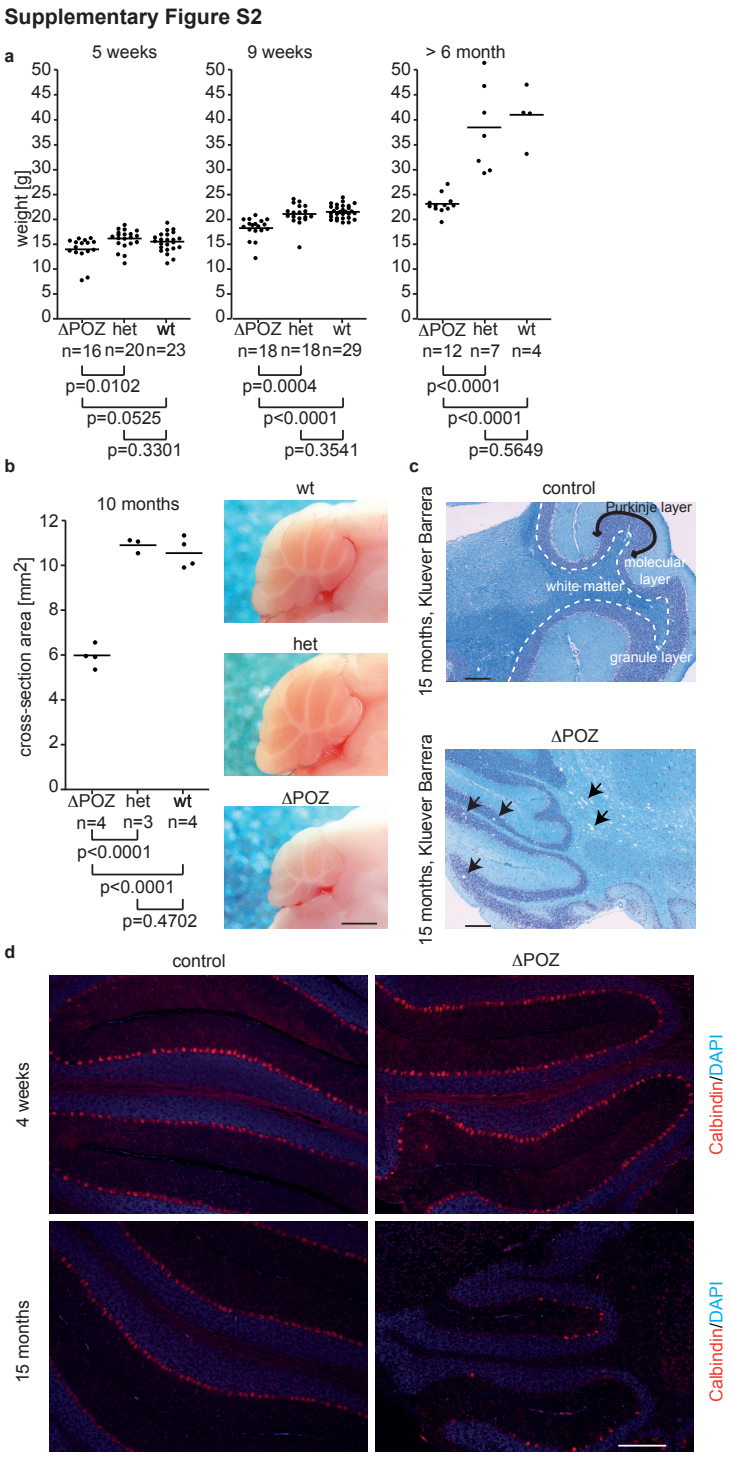

Supplementary Figure S2: *Miz1*$^{\Delta POZNes}$ mice develop a progressive neurodegenerative phenotype.

(a) Weight of *Miz1*$^{\Delta POZNes}$ mice and control mice at five and nine weeks as well as six months of age. All compared mice express the Nestin-Cre transgene. Data are shown for Miz1$^{\Delta POZNes}$ (Miz1$^{\Delta POZ/flox}$Cre^{+}, Miz1$^{flox/flox}$Cre^{+}), heterozygous (Miz1$^{+/\Delta POZ}$Cre^{+}, Miz1$^{+/flox}$Cre^{+}) and wild

type ($Miz1^{+/+}Cre^{+}$) mice. p-values were calculated using a two-tailed, unpaired t-test. The number of animals tested is shown below each graph.

(b) Defect of cerebellar growth in *Miz1*$^{\Delta POZNes}$ mice in comparison to wild type and heterozygous control mice. The panels show sagittal sections of brains at the age of 10 months. Scale bar: 1mm. Data are shown for $Miz1^{\Delta POZNes}$ ($Miz1^{\Delta POZ/flox}Cre^{+}$), heterozygous ($Miz1^{+/Flox}Cre^{+}$, $Miz1^{Flox/\Delta POZ}Cre^{-}$) and wild type ($Miz1^{+/+}Cre^{-}$) mice. p-values were calculated using a two-tailed, unpaired t-test. The number of animals tested is shown below each graph.

(c) Klüver-Barrera staining of cerebella from *Miz1*$^{\Delta POZNes}$ mice and control mice. Black arrows show perforations in the white matter and in the internal granular layer of *Miz1*$^{\Delta POZNes}$ mice. Scale bar: 200 μm.

(d) Immunofluorescence staining of Calbindin (Purkinje cells), nuclei are counterstained with DAPI. The age of mice is indicated. Scale bar: 200 μm.

Supplementary Figure S3

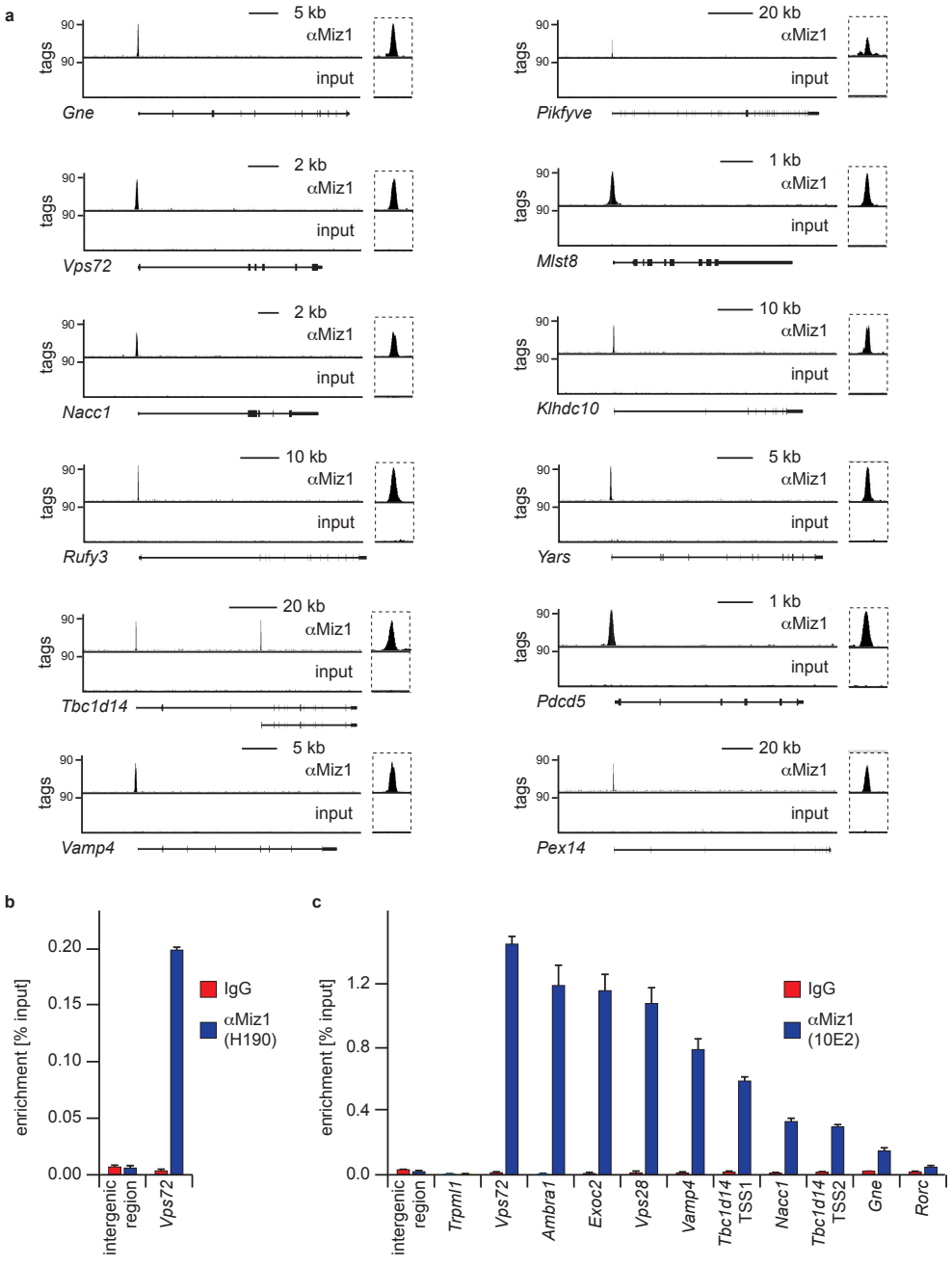

Supplementary Figure S3: Additional ChIP-Sequencing data.

(a) Additional examples of ChIP sequencing data obtained for Miz1. Input traces are shown as negative control. For each gene, the intron/exon structure is shown below the traces with

exons indicated as vertical bars and the transcriptional start site at the left. An enlarged picture of the peak region is shown on the right.

(b,c) Validation of the ChIP-sequencing results. Shown are data obtained with the antibody H190 (b, used in the ChIP-sequencing experiment) and 10E2 (c, a monoclonal α-Miz1 antibody). The immunoprecipitated material was analyzed by quantitative PCR at transcriptional start sites, which were positive for Miz1 binding in the ChIP-Sequencing experiment. An intergenic region and the transcriptional start site of *Trpml1* were used as negative controls. Error bars depict SD from three technical replicates.

Supplementary Figure S4

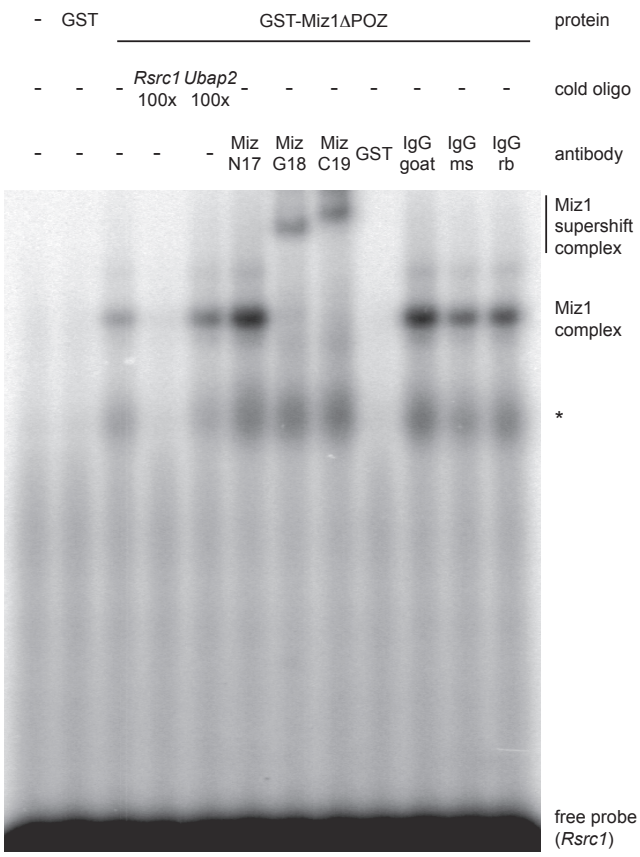

Supplementary Figure S4: DNA binding properties of recombinant Miz1.

Electrophoretic mobility shift assay (EMSA) analyzing binding of recombinant, purified GST-Miz1$^{\Delta POZ}$ to an oligonucleotide of the *Rsrc1* promoter spanning the motif identified by MEME-ChIP. An oligonucleotide spanning an E-box present in the *Ubap2* promoter was used as control. Competition was performed with a 100fold excess of non-labeled oligonucleotide as indicated. Supershift assays were carried out using two C-terminal Miz1 antibodies ("G18" and "C19") and a GST antibody. As controls we used IgG antibodies from different species as well as a Miz1 antibody ("N17") recognizing an N-terminal epitope not present in GST-Miz1$^{\Delta POZ}$. Shifts were reproduced three times and one representative result is shown. * indicates a lower migrating complex, which is compatible and disrupts after incubation with a GST antibody but not with C-terminal Miz1 antibodies, which therefore most likely results from truncated Miz1.

Supplementary Figure S5

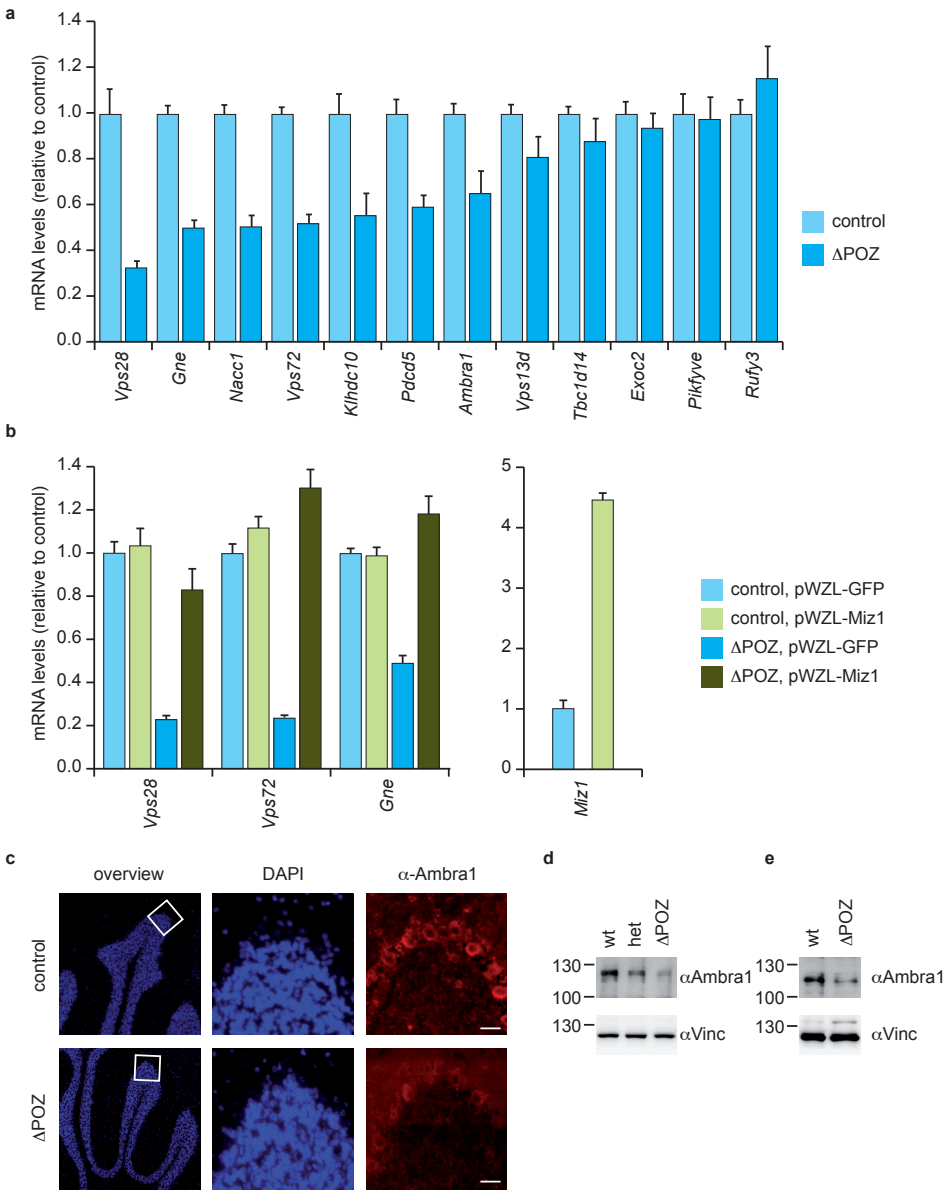

Supplementary Figure S5: Regulation of Miz1 target genes.

(a) qRT-PCR assays documented reduced expression of direct Miz1 target genes in *Miz1*$^{\Delta POZ}$ mouse embryonic fibroblasts (MEFs) in comparison to control MEFs. Error bars (SD) result from technical triplicates.

(b) Reduced expression of Miz1 target genes in *Miz1*$^{\Delta POZ}$ cells is rescued by expression of full-length Miz1. Mouse embryonic fibroblasts of the indicated genotypes were infected with retroviruses encoding full-length Miz1 or an empty vector control. The expression level of Miz1 target genes was measured by qRT-PCR. Error bars (SD) result from technical triplicates.

(c) Immunohistochemistry documenting expression of Ambra1 in cerebella of wild-type and *Miz1*$^{\Delta POZNes}$ mice at four weeks of age. Scale bar: 25 μm.

(d,e) Immunoblots of Ambra1 expression in (d) brains from *Miz1*$^{\Delta POZNes}$, heterozygous and wild type mice and (e) in wild type and Miz1$^{\Delta POZ}$ fibroblasts. Expression of α-vinculin was used as loading control.

Supplementary Figure S6

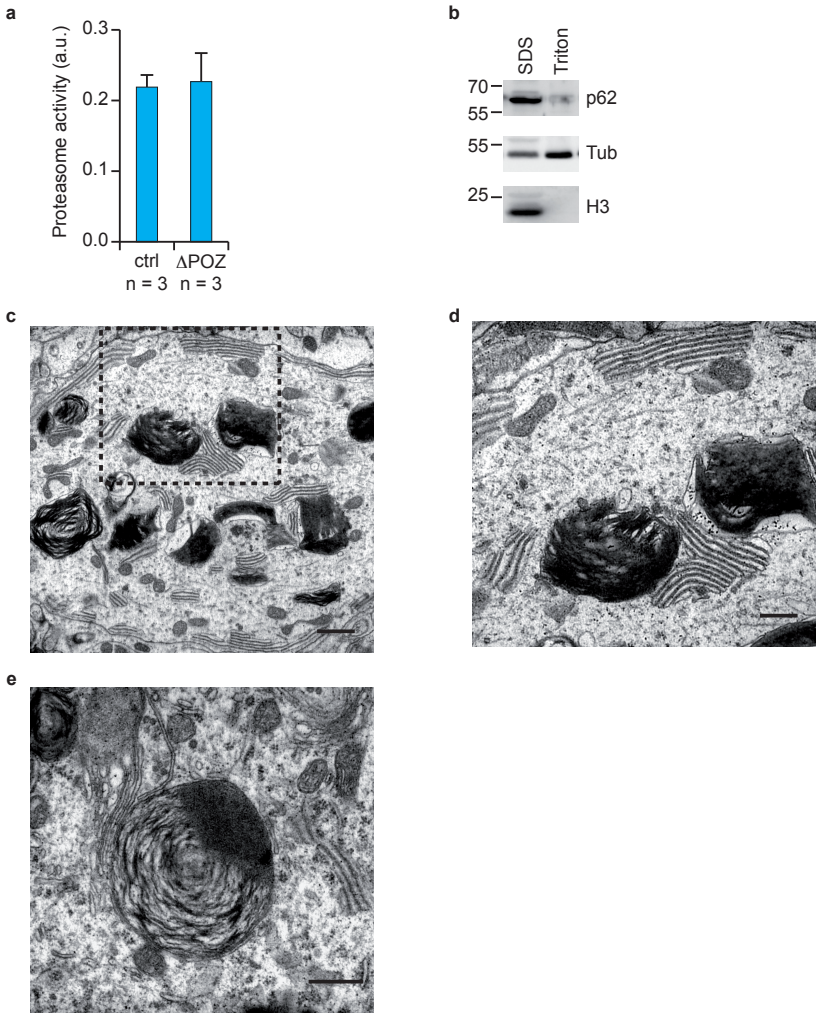

Supplementary Figure S6: Biochemical and ultrastructural analysis of *Miz1*$^{\Delta POZNes}$ mice.

(a) Proteasomal activity in cerebella of *Miz1*$^{\Delta POZNes}$ and control mice. Error bars represent SEM derived from the indicated numbers of animals.

(b) p62 accumulates in an insoluble manner in *Miz1*$^{\Delta POZNes}$ cerebella. Immunoblotting of p62 after sequential extraction of cerebellar proteins with TritonX-100 and SDS. α-tubulin and histone H3 were used as soluble/insoluble marker proteins.

(c-e) Transmission electron microscopic analysis of cerebella from aged *Miz1*$^{\Delta POZNes}$ mice. In the cytoplasm of Purkinje cells multilamellar bodies are found in close apposition (c,d: enlargement) and occasionally in contact (e) with cisterns of the endoplasmic reticulum. Scale bars: (c): 1000 nm, (d,e): 500nm.

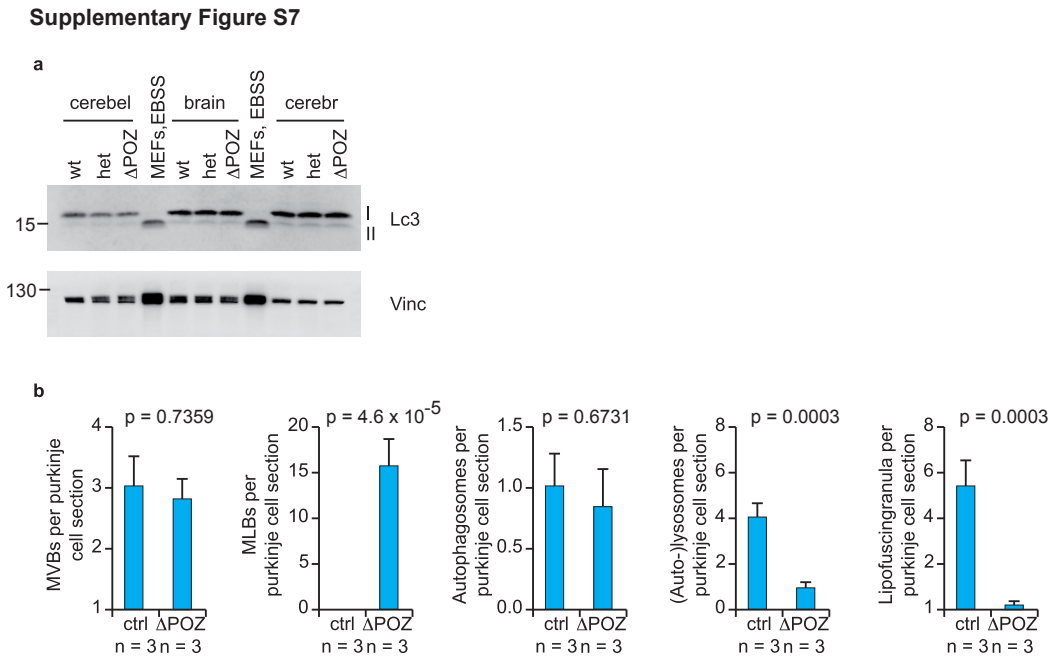

Supplementary Figure S7: Analysis of autophagy defects in cerebella from Miz1$^{\Delta POZNes}$ mice.

(a) Immunoblots documenting levels of unconjugated Lc3 and Lc3 conjugated to phosphatidylethanolamin (Lc3-II) in cerebella, total brain and cerebra of wild type, Miz1$^{\Delta POZNes}$ and heterozygous mice. As a positive control for conjugated Lc3, lysates from mouse embryo fibroblasts starved for amino acids ("MEFs, EBSS") were included as indicated.

(b) Quantification of different organelles in Purkinje cells of wild type and *Miz1*$^{\Delta POZNes}$ mice. The diagrams show the number of organelles found per section of an entire neuron. For each diagram, organelles in a minimum of 15 cells (n≥5 from 3 animals each) were counted. p-values were calculated using a two-tailed, unpaired t-test. Error bars show SEM. MVB-multivesicular bodies; MLB-multilamellar bodies.

Supplementary Figure S8

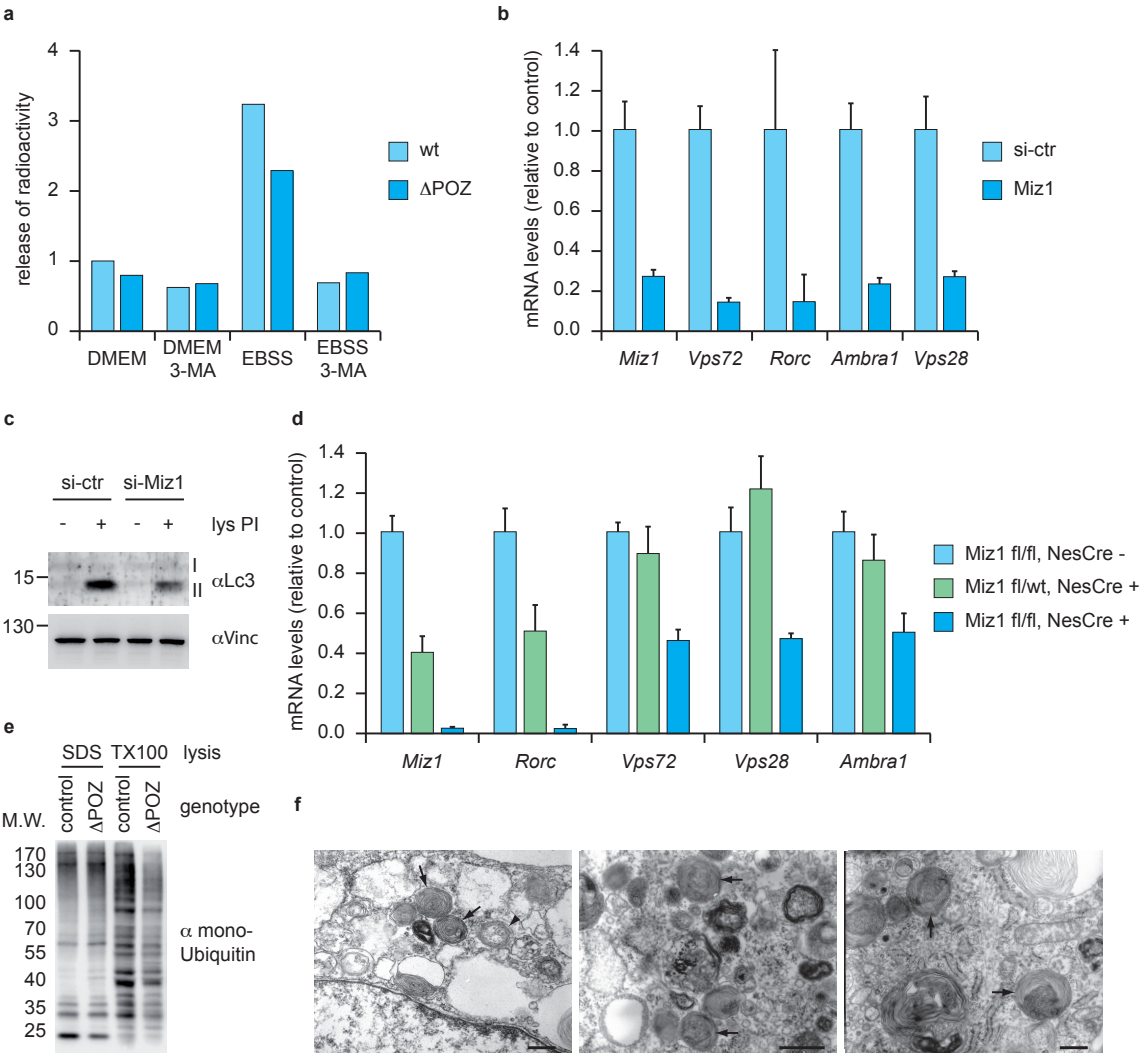

Supplementary Figure S8: Further characterization of Miz1$^{\Delta POZ}$ cells and neurospheres.

(a) Long-lived protein degradation assay in wild type and Miz1$^{\Delta POZ}$ mouse embryo fibroblasts. Where indicated, 3-methyladenin (3-MA) was added to inhibit autophagy. Values represent the average of two independent experiments with identical results.

(b) Acute depletion of Miz1 reduces expression of direct target genes. The graph shows the results of qRT-PCR assays analyzing expression of the indicated genes in mouse embryo fibroblasts transfected with siRNA targeting *Miz1* or control siRNA and harvested three days after transfection. Error bars depict SD of technical triplicates.

(c) Immunoblots using a α-Lc3 antibody detecting Lc3-I and conjugated Lc3-II. Mouse embryo fibroblasts were transfected with siRNA targeting *Miz1* or control siRNA as above. Where indicated, they were incubated with leupeptin and ammonium chloride (lys PI) for two hours in DMEM. The expression of α-vinculin (lower panels) was used as loading control.

(d) qRT-PCR assays documenting expression of *Miz1* and the indicated target genes of Miz1 in neurospheres isolated from mice of the indicated genotypes. Error bars depict SD of technical triplicates.

(e) Immunoblot of Triton X-100 soluble ("TX100") and insoluble ("SDS") fractions of lysates of cultured neuronal progenitor cells (NPCs) obtained from control and $Miz1^{\Delta POZ}$ mice. The blot was probed with an antibody recognizing mono-ubiquitinated proteins.

(f) Electron microscopy showing accumulation of multilamellar bodies (arrows; arrowhead: multivesicular body) in a subset of cells in $Miz1^{\Delta POZ}$ neurospheres. Some of these cells display large vacuoles, indicative of early stages of apoptosis. Scale bar: 0.5μm.

Supplementary Figure S9

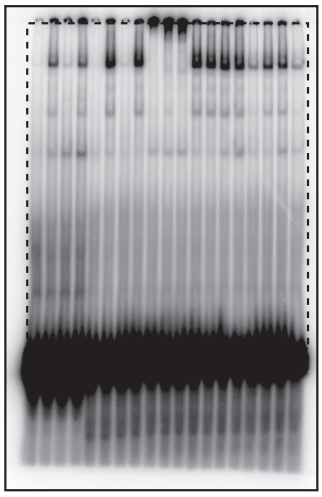

Figure 3 e

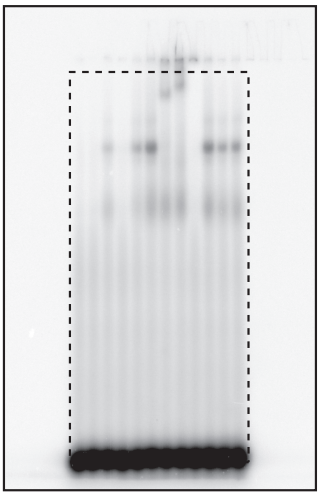

Figure S4

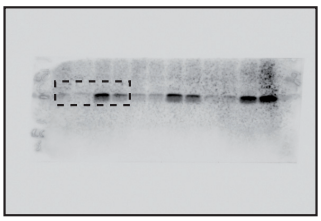

Figure 6 c-5

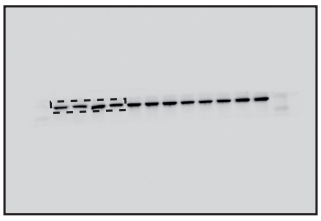

Figure 6 c-6

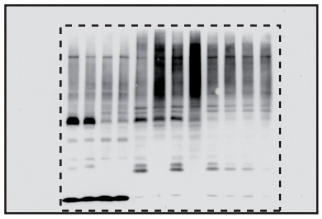

Figure 5 e-1

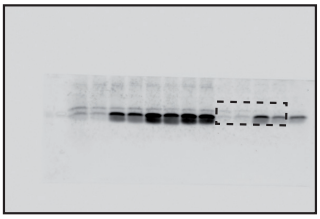

Figure 6 c-1

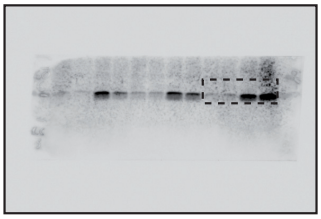

Figure 6 c-7

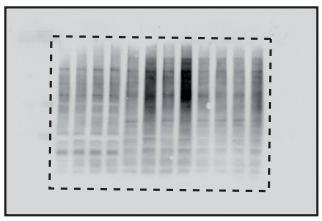

Figure 5 e-2

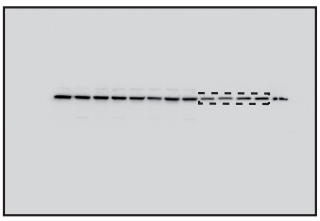

Figure 6 c-2

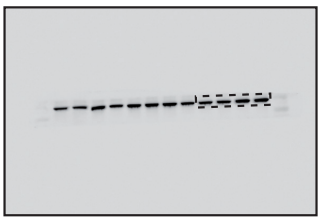

Figure 6 c-8

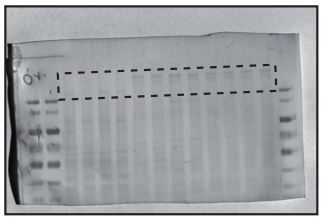

Figure 5 e-3

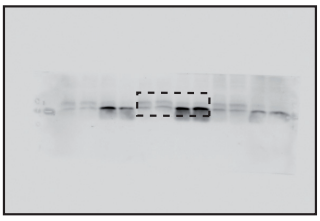

Figure 6 c-3

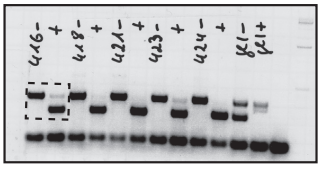

Figure 6 f

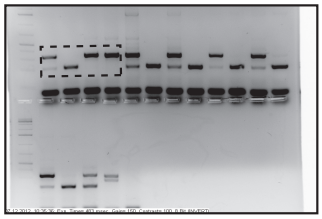

Figure 6 a

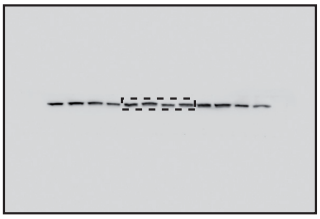

Figure 6 c-4

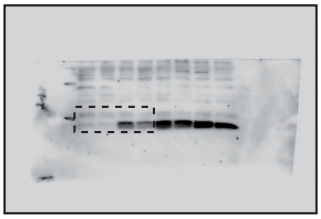

Figure 6 g-1

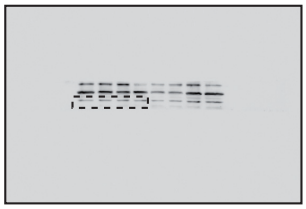

Figure 6 g-2

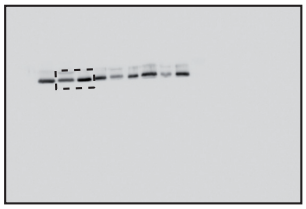

Figure S6 b-2

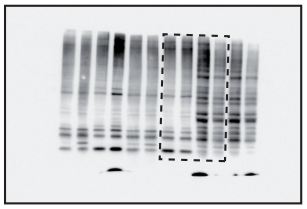

Figure S8 e

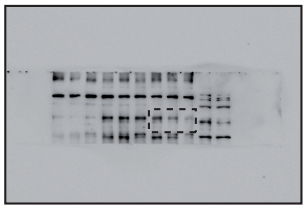

Figure S5 d-1

Figure S6 b-3

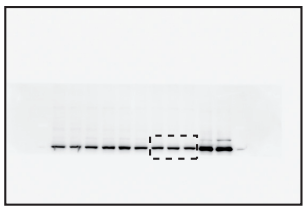

Figure S5 d-2

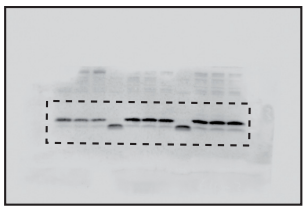

Figure S7 a-1

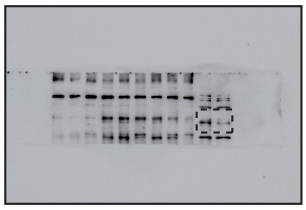

Figure S5 e-1

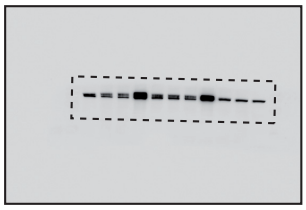

Figure S7 a-2

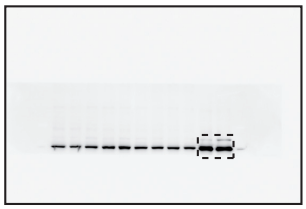

Figure S5 e-2

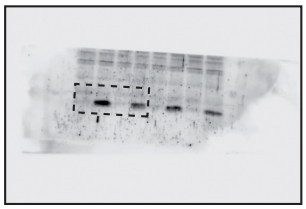

Figure S8 c-1

Figure S6 b-1

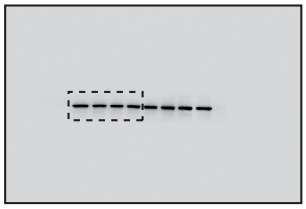

Figure S8 c-2

Supplementary Figure S9: Uncropped Images of all immunoblots.

Supplementary Table S1

alignment				
dataset	Input-NPC	Miz-NPC	input-MDA	Miz-MDA
high quality reads	35,940,222	36,008,514	12,681,385	15,837,713
aligned to	mm9	mm9	hg19	hg19
bowtie version	0.12.8	0.12.8	0.12.8	0.12.8
non-standard options	-m 1, -v 0	-m 1, -v 0		
aligned reads	27,282,985	26,383,298	12,070,466	14,321,677

peak annotation		
dataset	Miz-NPC	Miz-MDA
MACS-Version	1.4.2	1.4.2
treat	Miz-NPC	Miz-MDA
control	input-NPC	input-MDA
p-value	10^{-10}	10^{-10}
number of total peaks	261	2911
peaks in promotors (+/-1.5kb)	140	830
peaks in promotors after liftover to mm9	140	776

Supplementary Table S1: Parameter of next generation sequencing experiments.

The table lists the parameters of the individual sequencing experiments as well the parameters used for peak annotation.

Supplementary Table S2

gene symbol	tags	distance to next TSS
Abtb2	24	29110
Aff1	29	-481
Agxt2l2	20	-30032
Aip	183	3
Akap8l	284	-13941
Alox8	107	-13801
Ambra1	434	-21
Ank3	42	-143896
Arsk	246	-79
Atf6b	20	-150
Axin2	289	91556
Bahcc1	36	31436
Bcat1	33	17467
Bend5	104	-105
Bin1	17	-10523
C2cd5	297	-128
Cacna2d1	16	55194
Ccdc12	23	-210
Ccrn4l	111	-44788
Cct8	251	-124
Cdk8	178	29500
Cdk8	99	29361
Cdkl4	132	10447
Cenpe	46	-56996
Cep70	61	-56
Chd5	27	13310
Chsy3	17	148416
Clcc1	140	-3
Cmklr1	92	72815
Coa6	49	-42242
Cox19	331	-35
Cpped1	79	-69
Crybb3	29	-3920
Cstf1	376	-79
Ctgf	39	-10093
Cul2	31	-277
Dapp1	35	11403
Dcaf5	80	1396
Dclre1b	108	-20
Dcp1b	174	-80
Dctn6	299	5
Ddx18	78	-789
Dlg2	27	-390012
Dph1	269	-25

Dusp4	35	7045
Dync2h1	120	-51
Dynlrb1	70	-311
E130006D01Rik	52	-509
E130006D01Rik	26	828
E130307A14Rik	94	93
E2f7	152	58905
Eif2b3	292	-59
Entpd7	93	8178
Ercc2	332	-183
Erg	16	85669
Exoc2	325	-47
Fan1	407	-24
Fance	43	-128
Fbrsl1	65	-83
Fbxl15	84	189
Fbxl16	45	-5702
Fbxw5	95	25
Fgfr1op	50	11872
Fignl2	26	5864
Filip1l	349	38358
Fkbpl	143	-177
Gbe1	44	185
Gins3	209	-80
Gm12669	97	-35
Gm1821	24	-22772
Gm4559	87	-10448
Gm5464	23	10666
Gm6498	48	59213
Gm8579	217	-87017
Gm9054	27	1033
Gne	306	-39
Gphn	49	-531
Gtdc2	30	20508
Gtpbp8	68	-39
Hdac9	37	32815
Hdgf	294	-59
Heatr5a	310	-97
Hipk1	80	-39
Hipk2	90	-134
Hk1	45	19530
Hmgxb4	219	-49
Id1	88	5639
Idh1	102	-80
Ier5	42	116610
Ikzf2	84	-1278

Ikzf2	46	-1580
Impa2	18	6126
Ino80	248	-69
Kdm8	386	36
Kdr	34	53766
Kif26a	137	25666
Klhdc10	339	-178
Klhl5	16	-51228
Kras	112	-74
Lactb	122	-41
Limd1	140	-16713
Lrp12	263	-363
Lrtm1	31	11000
Lsm5	284	-81
Mettl25	287	-34
Mfsd6l	228	-19559
Mir146	20	103889
Mir297-1	23	-84965
Mir702	62	9428
Mlst8	330	1
Mmadhc	270	-73
Mn1	50	58234
Mrps15	305	39
Mrps23	316	-99
Msi1	27	-14469
Myom2	16	462281
Nacc1	198	-69
Ncam1	19	17465
Ncor2	43	58459
Ndufa5	228	65
Ngb	23	25680
Nrip1	35	22
Ogfod3	194	-38
Olfr1274-ps	80	-5480
Otud4	112	-117441
Palb2	388	-51
Parp1	42	-37
Pcbp1	20	9847
Pcdhgc5	58	57718
Pcnxl3	233	-167
Pdcd5	367	-70
Pde8b	26	21573
Pet117	245	-58
Pex1	254	133
Pex13	376	11
Pex14	267	-55

Pex16	238	-36
Pex2	265	-284475
Pgd	116	-121
Pip5k1a	39	-63
Pla2g15	106	-160
Pnma1	30	-13552
Poc1b	185	-344
Podn	250	-39337
Polr1c	25	953
Pomt1	304	-62
Pou4f1	18	131008
Ppap2b	36	62339
Prdm4	184	-259
Proc	38	20419
Psd3	78	-45820
Psd3	70	-39981
Psma1	329	2
Psmd3	370	-18
Psmg4	36	29
Ptcd1	277	-40
Ptpra	29	45852
Ptprm	22	-126208
Pts	34	-5336
Rad54l	109	-48
Raf1	267	69
Ranbp9	64	-593
Rasal2	238	-55
Rbm34	36	-8071
Rhbdd1	21	20067
Rif1	29	-81
Rmi2	17	33891
Rmnd5b	39	40
Rn45s	9148	2168
Rn45s	4096	4775
Rn45s	642	3610
Rn45s	398	4228
Rn45s	157	4061
Rn45s	142	3906
Rnf8	64	32
Rorc	52	-870
Rpl22	462	18
Rpl9	221	-54
Rps4y2	45	4016
Rsrc1	295	-17
Rufy3	305	-199
Rwdd1	263	-188

Sec16a	96	-679
Sec61g	27	-26530
Serpina4-ps1	140	-10291
Sfswap	19	-111540
Slit1	48	91684
Snord52	17	9562
Snrpa1	350	161
Snrpb2	259	-63
Snx18	333	-81
Soga2	28	86770
Sorcs1	19	293088
Sos1	202	-2663
Sos1	40	8809
Stxbp6	36	-363048
Suox	31	4491
Surf6	117	-220
Synj2	70	46141
Synj2	47	46002
Taf3	287	-29
Taf5l	109	-122
Taok3	386	-111
Tbc1d14	240	48
Tbc1d14	180	-45
Tbcb	81	12554
Tcea1	268	58
Tex2	248	-205
Tfdp2	77	-24
Thsd4	34	59054
Tiam2	19	-52602
Tmbim4	371	-84
Tmem167b	314	3
Tmem25	30	-57
Tpk1	118	-27
Tram1l1	26	-49
Trim27	44	-81
Tshz1	82	93
Tshz1	40	128087
Tshz2	45	-903
Tshz3	87	-1486
Tspan5	42	147199
Tsr2	137	-38
Ttc23	63	7958
Tug1	64	-38
Txndc11	119	-9588
U2surp	262	60
Ube3c	36	-84

Uqcc	44	1169
Vamp4	429	-296
Vav2	273	-15636
Vps13d	343	-43
Vps28	370	-101
Vps72	302	-34
Vti1a	68	170344
Vwf	43	32801
Wdr12	147	181
Wdr13	20	7
Yars	378	78
Yipf6	180	-331
Ypel2	22	72931
Zadh2	18	-533
Zdhhc15	23	203
Zdhhc21	34	169279
Zfp362	255	-5410
Zfp644	23	-68701
Zfyve20	233	-95
Zmiz2	55	-79
Znhit3	397	-98
1700001O22Rik	42	2029
1700018B08Rik	22	105022
1700034G24Rik	96	-71403
1810010D01Rik	40	95777
1810010D01Rik	27	67182
2900057B20Rik	33	7864
4930404N11Rik	29	3291
4930538K18Rik	22	-5605
4930546C10Rik	132	259396
6820431F20Rik	18	17647
9330133O14Rik	94	1009
9430038I01Rik	91	-76

Supplementary Table S2: List of Miz1 binding sites on chromatin in murine neurospheres.

The table lists the 261 peaks identified in the ChIP-Sequencing experiments, the number of tags found for each peak, the closest gene and the distance to the transcription start site.

Supplementary Table S3

gene symbol	description	direct Miz1 target gene	array sec. spheres control/ΔPOZ [logFC]	array quart. spheres control/ΔPOZ [logFC]	array young cer. control/ΔPOZ [logFC]	array old cer. control/ΔPOZ [logFC]	documented role in vesicular transport	reference	documented role in autophagy	reference
Rorc	RAR-related orphan receptor gamma	+	-3.98	-3.14	-2.58	-2.70	plays a role in lysosomal processing	[52]	knock down leads to accumulation of autophagosomes caused by impared lysosomal processing	[52]
Gne	glucosamine (UDP-N-acetyl)-2-epimerase/N-acetylmannosamine kinase	+	-1.03	-0.66	-2.09	-1.70			"rimmed vacuoles", which are caused by mutation or knockdown are clusters of autophagic vacuoles	[62]
Trpml1	mucolipin 1		-0.86	0.79	-0.11	-1.34	lysosomal transmembrane protein, which functions in the late endocytic pathway	[53]	required for neuronal macroautophagy	[28]
Vps72	vacuolar protein sorting 72	+	-0.23	-0.78	-0.33	-0.64	identified as a "vacular protein sorting" gene in yeast	[54]		
Vps13d	vacuolar protein sorting 13 D	+	-1.12	-1.14	-0.39	-0.62	identified as a "vacular protein sorting" gene in yeast	[54]		
Mlst8	MTOR associated protein, LST8 homolog	+	-0.08	0.46	-0.43	-0.60			component of mTorC1	[63]
Pikfyve	phosphoinositide kinase, FYVE finger containing	+	-0.04	0.26	-0.06	-0.58	regulates endomembrane homeostasis	[55]	necessary for maturation of autolysosomes	[31]
Rufy3	RUN and FYVE domain containing 3	+	-0.15	-0.25	-0.09	-0.55	mediates microtubule directed vesicle transport	[56]	direct interaction with autophagic components (LC3)	[56, 64]
Exoc2	exocyst complex component 2	+	-0.65	-0.70	-1.17	-0.50	essential for neuronal membrane trafficking and neurogenesis	[57]	part of the exocyst complex, exocyst components mediate autophagosome assambly	[65]
Ambra1	autophagy/beclin 1 regulator 1	+	-0.45	-0.61	-0.28	-0.49			regulates autophagy and development of nervous system	[30, 66]
Nacc1	nucleus accumbens associated 1, BEN and BTB (POZ) domain containing	+	0.02	-0.10	-0.19	-0.49			regulates stress-induced autophagy	[67, 68]
Vps28	vacuolar protein sorting 28	+	-0.60	-0.73	-0.58	-0.38	member of ESCRT-I, sorting of ubiquitinated proteins in multivesicular body/late endosome pathway	[58, 19]	ESCRTs regulate autophagy; ESCRT plays role in autophagy associated neurodegeneration	[31, 69]
Klhdc10	kelch domain containing 10	+	0.04	0.00	-0.07	-0.19			direct interaction with autophagic components	[64]
Tbc1d14	TBC1 domain family, member 14	+	-0.19	-0.29	-0.26	-0.07	regulates recycling endosomal trafficking	[59]	regulates starvation-induced autophagy	[70]
Pdcd5	programmed cell death 5	+	0.12	-0.11	-0.14	-0.04			activator of autophagy	[71]
Vamp4	vesicle-associated membrane protein 4	+	-0.53	-0.56	-0.33	-0.03	plays a role in trans-Golgi network-to-endosome transport	[60]	was found in phagocytotic membranes together with LC3, induction of autophagy leads to strong enrichment of Vamp4	[72]
Pex14	peroxisomal biogenesis factor 14	+	-0.17	0.12	0.08	0.00	peroxisomal membrane protein	[61]	required for peroxisomal autophagy (pexophagy)	[73]

Supplementary Table S3: Miz1 target genes with documented roles in autophagy.

The table summarizes microarray data, previously published data linking proteins encoded by Miz1 target genes to autophagy and relevant literature.

Supplementary Table S4

GO term	p-value sec. spheres	q-value sec. spheres	p-value quart. spheres	q-value quart. spheres
cell morphogenesis involved in differentiation	> 0.1	1	1.4×10^{-5}	0.030
neuron projection morphogenesis	> 0.1	1	1.5×10^{-4}	0.065
neuron differentiation	> 0.1	1	1.8×10^{-4}	0.055
axogenesis	> 0.1	1	2.1×10^{-4}	0.057

Supplementary Table S4: Microarray analysis of secondary and quaternary *Miz1*$^{\Delta POZ}$ and control neurospheres was performed. Genes that are downregulated more than twofold in quarternary *Miz1*$^{\Delta POZ}$ neurospheres were subjected to GO-term analysis. The table lists p- and q-values for individual GO-terms in secondary and quarternary spheres (http://david.abcc.ncifcrf.gov/home.jsp).

Supplementary Table S5

Rank	geneset	NES	p-value	q-value
1	Schuhmacher Myc Targets up	3.08	0.000	0.000
4	Dang Myc Targets up	2.82	0.000	0.000
6	Coller Myc Targets up	2.75	0.000	0.000
17	Menssen Myc Targets	2.41	0.000	0.000
391	Miz-bound Promotors NPC	0.75	0.969	1.000

Supplementary Table S5: Lack of regulation of Miz1-autophagic target genes by Myc.

The panel shows the results of a GSEA demonstrating using a dataset from T-cell lymphomas that express a doxycyclin-regulatable allele of Myc[2]. Microarrays were performed before and 24hrs after de-induction of Myc. The table documents significant regulation of known sets of Myc-target genes and the lack of significant regulation of the gene set which contains the 140 genes directly bound by Miz1 (see Figure 3c).

Supplementary Table S6

Supplementary Table S6	
qRT-PCRs:	**sequence**
Miz-1 for	CGTGGTGCACCTAGACATCA
Miz-1 rev	GTTCTCAGGGCTAAGGCTCA
Cdkn2b (p15) for	TGCAGATGATCCACAGGCTA
Cdkn2b (p15) rev	GTGAATCCCCACACATGACA
Cdkn1a (p21) for	TCCACAGCGATATCCAGACA
Cdkn1a (p21) rev	GGCACACTTTGCTCCTGTG
Cdkn1c (p57) for	CAGGACGAGAATCAAGAGCA
Cdkn1c (p57) rev	GCTTGGCGAAGAAGTCGT
Cdkn2a (p16) for	AACGCCCCGAACTCTTTC
Cdkn2a (p19) for	GCTCTGGCTTTCGTGAACAT
Cdkn2a (p19) rev	GTGAACGTTGCCCATCATC
Myc for	TTTGTCTATTTGGGGACAGTGTT
Myc rev	CATCGTCGTGGCTGTCTG
Bmi1 for	AAACCAGACCACTCCTGA
Bmi1 rev	TCTTCTTCTCTTCATCTCA
Gne for	CAAACCTGAGGGTGGCAATA
Gne rev	GGTTTTAGGGTTGAACTGAGTG
Rorc for	ACCTCTTTTCACGGGAGGA
Rorc rev	TCCCACATCTCCCACATTG
Exoc2 for	GGGAGAACCTGGGTACTGGT
Exoc2 rev	CCGTGAGGAGGCAATTATGT
Vps72 for	GGAGGCCAAGATCACTGAAG
Vps72 rev	CAGCCTCCAGCCTTTCATAG
Vps28 for	AGCTTCTGTCGCCATCTCC
Vps28 rev	CCCAGGCAGCTATACAGCAC
Vps13d for	CTGTCGGTTGCACTTCTCAA
Vps13d rev	GGCTACGATCAGGCAGAATC
Ambra1 for	GAGCACCCAATTTACCCAGA
Ambra1 rev	GATCATCCTCTGGGCGTAGTA
Nacc1 for	GTGACCCCTCAGAGAAGCTG
Nacc1 rev	TGGCAGTTCATAAGCTGTGC
Pikfive for	CCCCCTTCAAGTCAGCATATAG
Pikfive rev	GAGACTGCTGCTCTCCTTGG
Rufy3 for	TGATGCAAAAGAAGCTTTCTGA
Rufy3 rev	TGAGGGCATTGACTTCATAGA
Pdcd5 for	TCAGCCAACAGACAGAAAAGAA
Pdcd5 rev	CGTCTTCATCGGAGTCCATT
Tbc1d14 for	CAAAGCCGGAACAAGAAATG
Tbc1d14 rev	GGCTTCCTTTCTCCATCTCC
Klhdc10 for	CCAGATGGGTACAGATGGCTA
Klhdc10 rev	AGGTTGTTTCCATGCAGCAC
Pex14 for	CCAGGAAGTGAAAATGTGGTG
Pex14 rev	GGACCCGAGAATTCTGTAGGA
RpS16 for	AGGAGCGATTTGCTGGTGTG
RpS16 rev	GCTACCAGGGCCTTTGAGAT
Actb for	CTAAGGCCAACCGTGAAAAG
Actb rev	ACCAGAGGCATACAGGGACA
Beta2m for	AGCCGAACATACTGAACTGCTACG

Beta2m rev	CGGCCATACTGTCATGCTTAACTC
genomic PCRs:	
Miz-1 intron 2	GTATTCTGCTGTGGGGCTATC
Miz-1 exon 3	GGCTGTGCTGGGGGAAATC
Miz-1 intron 4	GGCAGTTACAGGCTCAGGTG
Cre Nestin for	CCGTTTGCCGGTCGTGGG
Cre Nestin rev	CGTATATCCTGGCAGCGATC
Vps72-TSS for	AGACGCTGAACTTCCGTCAT
Vps72-TSS rev	CAGATCGGCACTCGACACTA
Vamp4-TSS for	AGACGCTCGATCTCCGTTG
Vamp4-TSS rev	TACTCCGAGTCCTGGAGAGG
Vps28-TSS for	CGCAAGCTCAGGCAAAAA
Vps28-TSS rev	AGCTCGGCACTCATCCTCTA
Ambra1-TSS for	AGCAGGAGCTGAGCAATGTT
Ambra1-TSS rev	GCCCAGACATCAAAGGAAGA
Exoc2-TSS for	ACTCGGTGCTCGGCTAGG
Exoc2-TSS rev	AGCACTAGGGCCGCACTT
Rorc-TSS for	GGTTGTTGGGTAAGCAGGAA
Rorc-TSS rev	AATATTGGATGCCTCAGTTCG
Gne-TSS for	ACTACCAGAGGCGACACGAC
Gne-TSS rev	CCCCTCCTTGGCGTATTT
Nacc1-TSS for	AAAGAGGAGCTGGTGAGAACC
Nacc1-TSS rev	GGCAGGGAGGAAAACTGC
Tbc1d14-TSS1 for	ATGATCTGTAACCTGCGCTCAC
Tbc1d14-TSS1 rev	AGCAGCTGGGGGAGTCTTA
Tbc1d14-TSS2 for	GCCCAACCTAGGAACACTGA
Tbc1d14-TSS2 rev	GAACGGCAGGACACTCAATC
Mcoln1-TSS for	CGCTTGTCACGTGTTCAGTT
Mcoln1-TSS rev	CTTCAAACCCTCCCGCATC
intergenic for	CACAAGTGTGGAGCCTGGTA
intergenic rev	CCTTGAACTTGCAGCTTTCC
EMSA:	
Vps28 for	GCTACTCCAGAGCGCAAGCTCAGGCAAAAAAAGCC GAGTGCCGATCAATGGATTTGGCTTGCT
Vps28 rev	AGCAAGCCAAATCCATTGATCGGCACTCGGCT TTTTTTGCCTGAGCTTGCGCTCTGGAGTAGC
Ambra1 for	GCTGAGCAATGTTTCGGCACTCGGCTGCAGTG CCTTGAACGATTGCTGGGGCGCTCTTCCT
Ambra1 rev	AGGAAGAGCGCCCCAGCAATCGTTCAAGGCACTGC AGCCGAGTGCCGAAACATTGCTCAGC
*Rsrc1*wt for	GTCCATCGATGCACTCGATATCTCGGCTGAAGCTG CCTGGCGCTAGAACCAGGAAGGCGC
*Rsrc1*wt rev	GCGCCTTCCTGGTTCTAGCGCCAGGCAGCTTCAGC CGAGATATCGAGTGCATCGATGGAC
*Rsrc1*mut1 for	GTCCATCGATGCACGAGATATCTCGGCTGAAGCTG CCTGGCGCTAGAACCAGGAAGGCGC
*Rsrc1*mut1 rev	GCGCCTTCCTGGTTCTAGCGCCAGGCAGCTTCAGC CGAGATATCTCGTGCATCGATGGAC
*Rsrc1*mut4 for	GTCCATCGATGCACGAGATATCGATGAGGAAGCTG CCTGGCGCTAGAACCAGGAAGGCGC

*Rsrc1*mut4 rev	GCGCCTTCCTGGTTCTAGCGCCAGGCAGCTTCCTC ATCGATATCTCGTGCATCGATGGAC
*Rsrc1*mut5 for	GTCCATCGATGCACTCGATATATCGGCTGAAGCTG CCTGGCGCTAGAACCAGGAAGGCGC
*Rsrc1*mut5 rev	GCGCCTTCCTGGTTCTAGCGCCAGGCAGCTTCAGC CGATATATCGAGTGCATCGATGGAC
Ubap2 for	GGCTTGCCCTGAGTGGTTGGACCACATCACGTGAT GAGCACAGGGCGGCCACAGGGGAGT
UBAP2 rev	ACTCCCCTGTGGCCGCCCTGTGCTCATCACGTGAT GTGGTCCAACCACTCAGGGCAAGCC
cloning:	
RORC for	CCGCTCGAGAGAGCAGGAGGAGGTGCCAG
RORC rev	GGAAGATCTGGGGCAGCTCCCTTGGTGCC
AMBRA1 for	CCGCTCGAGAGTAGGAGTTGAGCTGTTTT
AMBRA1 rev	GGAAGATCTCAAAGGAGGAACGCCCAAGC

Supplementary Table S6: Primer Sequences.

Supplementary References

52 Lipinski, M. M. *et al.* A genome-wide siRNA screen reveals multiple mTORC1 independent signaling pathways regulating autophagy under normal nutritional conditions. *Dev Cell* **18**, 1041-1052 (2010).

53 Thompson, E. G., Schaheen, L., Dang, H. & Fares, H. Lysosomal trafficking functions of mucolipin-1 in murine macrophages. *BMC Cell Biol* **8**, 54 (2007).

54 Bankaitis, V. A., Johnson, L. M. & Emr, S. D. Isolation of yeast mutants defective in protein targeting to the vacuole. *Proc Natl Acad Sci U S A* **83**, 9075-9079 (1986).

55 Rutherford, A. C. *et al.* The mammalian phosphatidylinositol 3-phosphate 5-kinase (PIKfyve) regulates endosome-to-TGN retrograde transport. *J Cell Sci* **119**, 3944-3957 (2006).

56 Pankiv, S. *et al.* FYCO1 is a Rab7 effector that binds to LC3 and PI3P to mediate microtubule plus end-directed vesicle transport. *J Cell Biol* **188**, 253-269 (2010).

57 Murthy, M., Garza, D., Scheller, R. H. & Schwarz, T. L. Mutations in the exocyst component Sec5 disrupt neuronal membrane traffic, but neurotransmitter release persists. *Neuron* **37**, 433-447 (2003).

58 Rieder, S. E., Banta, L. M., Kohrer, K., McCaffery, J. M. & Emr, S. D. Multilamellar endosome-like compartment accumulates in the yeast vps28 vacuolar protein sorting mutant. *Mol Biol Cell* **7**, 985-999 (1996).

59 Longatti, A. & Tooze, S. A. Recycling endosomes contribute to autophagosome formation. *Autophagy* **8**, 1682-1683 (2012).

60 Mallard, F. *et al.* Early/recycling endosomes-to-TGN transport involves two SNARE complexes and a Rab6 isoform. *J Cell Biol* **156**, 653-664 (2002).

61 Komori, M. *et al.* The Hansenula polymorpha PEX14 gene encodes a novel peroxisomal membrane protein essential for peroxisome biogenesis. *Embo J* **16**, 44-53 (1997).

62 Malicdan, M. C. V., Noguchi, S. & Nishino, I. Autophagy in a mouse model of distal myopathy with rimmed vacuoles or hereditary inclusion body myopathy. *Autophagy* **3**, 396-398 (2007).

63 Sini, P., James, D., Chresta, C. & Guichard, S. Simultaneous inhibition of mTORC1 and mTORC2 by mTOR kinase inhibitor AZD8055 induces autophagy and cell death in cancer cells. *Autophagy* **6**, 553-554 (2010).

64 Behrends, C., Sowa, M. E., Gygi, S. P. & Harper, J. W. Network organization of the human autophagy system. *Nature* **466**, 68-76 (2010).
65 Bodemann, B. O. *et al.* RalB and the exocyst mediate the cellular starvation response by direct activation of autophagosome assembly. *Cell* **144**, 253-267 (2011).
66 Vazquez, P. *et al.* Atg5 and Ambra1 differentially modulate neurogenesis in neural stem cells. *Autophagy* **8**, 187-199 (2012).
67 Zhang, Y., Yang, J. W., Ren, X. & Yang, J.-M. NAC1 and HMGB1 enter a partnership for manipulating autophagy. *Autophagy* **7**, 1557-1558 (2011).
68 Zhang, Y. *et al.* NAC1 modulates sensitivity of ovarian cancer cells to cisplatin by altering the HMGB1-mediated autophagic response. *Oncogene* **31**, 1055-1064 (2012).
69 Lee, J.-A. & Gao, F.-B. Roles of ESCRT in autophagy-associated neurodegeneration. *Autophagy* **4**, 230-232 (2008).
70 Longatti, A. *et al.* TBC1D14 regulates autophagosome formation via Rab11- and ULK1-positive recycling endosomes. *J Cell Biol* **197**, 659-675 (2012).
71 An, L. *et al.* Involvement of autophagy in cardiac remodeling in transgenic mice with cardiac specific over-expression of human programmed cell death 5. *PLoS One* **7**, e30097 (2012).
72 Shui, W. *et al.* Membrane proteomics of phagosomes suggests a connection to autophagy. *Proc Natl Acad Sci U S A* **105**, 16952-16957 (2008).
73 Zutphen, T. v., Veenhuis, M. & van der Klei, I. J. Pex14 is the sole component of the peroxisomal translocon that is required for pexophagy. *Autophagy* **4**, 63-66 (2008).